

# Transition of Magnetic Reconnection Regimes in Partially Ionized Plasmas

LIANG WANG <sup>1</sup> CHUANFEI DONG <sup>1,2</sup> YI-MIN HUANG <sup>3,4</sup> YUE YUAN <sup>1,5</sup> XINMIN LI <sup>1</sup> AND YANG ZHANG <sup>6,7</sup>

<sup>1</sup>Center for Space Physics and Department of Astronomy, Boston University, Boston, MA 02215, USA

<sup>2</sup>School of Natural Sciences, Institute for Advanced Study, Princeton, NJ 08540, USA

<sup>3</sup>Department of Astronomy, University of Maryland, College Park, Maryland 20742, USA

<sup>4</sup>National Aeronautics and Space Administration Goddard Space Flight Center, Greenbelt, MD 20771, USA

<sup>5</sup>Department of Earth, Planetary, and Space Sciences, University of California, Los Angeles, Los Angeles, CA, 90095, USA

<sup>6</sup>Department of Astrophysical Sciences, Princeton University, Princeton, NJ 08544, USA

<sup>7</sup>University Corporation for Atmospheric Research, Boulder, CO 80301, USA

## ABSTRACT

Magnetic reconnection in partially ionized plasmas plays a crucial role in a wide range of solar, astrophysical, and laboratory environments. While reconnection in such plasmas is commonly characterized by the ion-neutral coupling strength and the ionization fraction  $\chi = n_i/(n_i + n_n)$ , most previous studies have focused primarily on the former. A systematic exploration of the ionization fraction, particularly in combination with ion-neutral coupling, is still lacking. This study presents the first systematic scan of the two-dimensional parameter space defined by ion-neutral collisionality and ionization fraction, enabling investigation of the transition from strongly coupled reconnection to faster, decoupled reconnection. To achieve this, we employ a new three-fluid, five-moment numerical model that treats electrons, ions, and neutrals as separate species on an equal footing. We find that in the strongly coupled regime, the reconnection rate is consistent with a  $\chi^{1/4}$  scaling. As collisionality decreases, the system transitions to a fast, ionization-independent regime. On the other hand, in all simulations, the current sheet thins down to the ion inertial length  $d_i$ , rather than the expanded hybrid scale  $d_i\chi^{-1/2}$  predicted by analytic fluid theories. The identified critical thickness and the resulting onset of fast reconnection agree reasonably well with recent fully kinetic simulations and laboratory experiments. In addition, we show that, over a wide range of coupling strengths, the ion outflow velocities remain Alfvénic, scaling with the appropriate ion or hybrid Alfvén speed, while the hybrid outflow velocity scales as  $\chi^{1/2}$  when normalized by ion Alfvén speed.

## 1. INTRODUCTION

Magnetic reconnection is a fundamental plasma process characterized by the breaking and topological reconnection of magnetic field lines, facilitating the rapid conversion of magnetic energy into kinetic and thermal energy (E. G. Zweibel & M. Yamada 2009; M. Yamada et al. 2010; H. Ji et al. 2022). While historically studied in fully ionized regimes, reconnection is common in partially ionized plasmas, such as the solar chromosphere (K. Shibata et al. 2007; H. Tian et al. 2014; L. Ni et al. 2020), protostellar disks (K. I. Öberg et al. 2011), and the interstellar medium (D. B. Fielding et al. 2023). In these environments, interactions between charged particles and neutrals can strongly influence the structure of the current sheet and modify both the onset criteria and the rate of energy dissipation.

Theories for reconnection in partially ionized plasmas are often defined by the coupling regimes between ions and neutrals: weak, intermediate, or strong cou-

pling (E. G. Zweibel 1989; L. M. Malyskhin & E. G. Zweibel 2011). In the strongly coupled limit, where the ion-neutral collision frequency  $\nu_{in}$  is high relative to the transit time through the current sheet, ions and neutrals move together, effectively increasing the bulk inertia by a factor of  $\chi$ , defined as the ionization fraction  $\chi = n_i/(n_i + n_n)$ , where  $n_i$  and  $n_n$  are the ion and neutral densities, respectively. One immediate consequence is the slowdown of the bulk Alfvén speed, and thus the Lundquist number is reduced, by a factor of  $\chi^{1/2}$ . The steady-state resistive Sweet-Parker reconnection rate, normalized over the ion Alfvén speed, is correspondingly reduced by a factor of  $\chi^{1/4}$ , while the Sweet-Parker current sheet thickness is thickened to  $\delta_{SP}^* = \chi^{-1/4}\delta_{SP}$ . On the other hand, the enhanced inertia also leads to the broadening of the inertial length  $d_i$  by a factor of  $\chi^{-1/2}$  to  $d_i^* = \chi^{-1/2}d_i$ . It was predicted that reconnection would transition to a fast regime once the Sweet-Parker current sheet thins to the hybrid inertial length.

Recent studies showed interesting discrepancies between predictions from fully coupled fluid models and results from kinetic approaches. Laboratory experiments at MRX (E. E. Lawrence et al. 2013) and fully kinetic Particle-In-Cell (PIC) simulations (J. Jara-

Corresponding author: Liang Wang

Corresponding author: Chuanfei Dong

Almonte et al. 2019) indicate that the current sheet thickness does not expand to the hybrid inertial length  $d^*$  but rather stays at ion inertial length  $d_i$ , regardless of the ionization fraction. The comparative study of J. Jara-Almonte et al. (2021) further found that multi-fluid MHD simulations tend to maintain a coupled state and produce a slower, Sweet-Parker-like scaling. In contrast, at higher ionization fraction ( $\chi > 0.15$ ), fully kinetic simulations allow a transition to faster, decoupled reconnection, where the reconnection rate scales like  $\chi^{1/2}$  when normalized using the Alfvén speed based on the ion mass density  $\rho_i$ , indicating fast reconnection rate at the bulk Alfvén speed.

The discrepancies noted above point to a gap between fluid and kinetic descriptions. In this study, we address this gap using a five-moment, three-fluid model that treats electrons, ions, and neutrals as separate species. We scan ion-neutral collisionality and ionization fraction to identify the transition from strongly coupled, resistive reconnection to decoupled, Hall-mediated reconnection. We then compare the resulting reconnection behavior with earlier kinetic and multifluid MHD results to evaluate whether the five-moment model can capture the onset, rate, and current-sheet structure of fast reconnection seen in kinetic regimes. We do not include charge exchange, ionization, or recombination, as our goal is to isolate the role of frictional coupling between ions and neutrals.

The paper is structured as follows: Sec. 2 details the numerical model and the simulation setup employed in this study; Sec. 3 presents the primary simulation results; in Sec. 4, we further discuss the findings and their broader implications.

## 2. NUMERICAL MODEL AND SIMULATION SETUP

The Gkeyll five-moment multifluid model (A. Hakim et al. 2006; L. Wang et al. 2020) is used in this study. This model evolves the density, momentum, and energy equations of electron, ion, and neutral species (denoted by subscripts  $e$ ,  $i$ , and  $n$ ) separately. The number density equations take the form

$$\frac{\partial(m_s n_s)}{\partial t} + \nabla \cdot (m_s n_s \mathbf{u}_s) = 0, \quad s = e, i, n, \quad (1)$$

where  $m_s$ ,  $n_s$ , and  $\mathbf{u}_s$  are the mass, number density, and bulk velocity of species  $s$ . The momentum equations are

$$\frac{\partial(m_e n_e \mathbf{u}_e)}{\partial t} + \nabla \cdot (m_e n_e \mathbf{u}_e \mathbf{u}_e) + \nabla p_e \quad (2)$$

$$= n_e q_e (\mathbf{E} + \mathbf{u}_e \times \mathbf{B}) + \mathbf{R}_{ei},$$

$$\frac{\partial(m_i n_i \mathbf{u}_i)}{\partial t} + \nabla \cdot (m_i n_i \mathbf{u}_i \mathbf{u}_i) + \nabla p_i \quad (3)$$

$$= n_i q_i (\mathbf{E} + \mathbf{u}_i \times \mathbf{B}) + \mathbf{R}_{in} + \mathbf{R}_{ie},$$

$$\frac{\partial(m_n n_n \mathbf{u}_n)}{\partial t} + \nabla \cdot (m_n n_n \mathbf{u}_n \mathbf{u}_n) + \nabla p_n = \mathbf{R}_{ni}. \quad (4)$$

where  $q_s$  is the charge of species  $s$ . In particular,  $q_n = 0$ ,  $q_i = -q_e = e$ . The ion-neutral and neutral-ion collision terms are formulated to conserve total momentum between the two species,

$$\mathbf{R}_{in} = \nu_{in} n_i m_i (\mathbf{u}_n - \mathbf{u}_i), \quad (5)$$

$$\mathbf{R}_{ni} = \nu_{ni} n_n m_n (\mathbf{u}_i - \mathbf{u}_n), \quad (6)$$

where the collision frequency is calculated during the simulation by

$$\nu_{in} = \Sigma_{in} \sqrt{\frac{8k_B T_{in}}{\pi m_{in}}} \frac{n_n m_n}{m_n + m_i}, \quad (7)$$

$$\nu_{ni} = \Sigma_{in} \sqrt{\frac{8k_B T_{in}}{\pi m_{in}}} \frac{n_i m_i}{m_n + m_i}, \quad (8)$$

with  $\Sigma_{in} = \Sigma_{ni}$  being the collisional cross-section of choice,  $m_{ni} = m_{in} \equiv m_i m_n / (m_i + m_n)$  being the reduced mass, and  $T_{in} = T_{ni} \equiv (m_i T_n + m_n T_i) / (m_i + m_n)$  being the reduced temperature. For this study,  $\Sigma_{in}$  is a constant. The friction terms between electrons and ions are similarly defined.

Finally, the energy equations take the form

$$\frac{\partial \mathcal{E}_e}{\partial t} + \nabla \cdot [\mathbf{u}_e (p_e + \mathcal{E}_e)] = n_e q_e \mathbf{u}_e \cdot \mathbf{E} + Q_{ei}, \quad (9)$$

$$\frac{\partial \mathcal{E}_i}{\partial t} + \nabla \cdot [\mathbf{u}_i (p_i + \mathcal{E}_i)] = n_i q_i \mathbf{u}_i \cdot \mathbf{E} + Q_{in} + Q_{ie}, \quad (10)$$

$$\frac{\partial \mathcal{E}_n}{\partial t} + \nabla \cdot [\mathbf{u}_n (p_n + \mathcal{E}_n)] = Q_{ni}, \quad (11)$$

where  $\mathcal{E}_s = \frac{p_s}{\gamma-1} + \frac{1}{2} m_s n_s |\mathbf{u}_s|^2$  is the total (internal plus kinetic) energy,  $\gamma = 5/3$ , and  $p_s$  is the species' scalar pressure, and the heating terms are

$$Q_{in} = \frac{n_i m_i \nu_{in}}{m_i + m_n} \left[ 2 \left( \frac{p_n}{n_n} - \frac{p_i}{n_i} \right) + \frac{1}{3} m_i |\mathbf{u}_n - \mathbf{u}_i|^2 \right], \quad (12)$$

$$Q_{ni} = \frac{n_n m_n \nu_{ni}}{m_i + m_n} \left[ -2 \left( \frac{p_n}{n_n} - \frac{p_i}{n_i} \right) + \frac{1}{3} m_n |\mathbf{u}_n - \mathbf{u}_i|^2 \right]. \quad (13)$$

The heating due to electron-ion collisions are implemented similarly. Note that the momentum transfer and heating formulations adopted here assume elastic Maxwell molecule collisions. More detailed and further variants of the fluid collision equations can be found in R. Schunk & A. Nagy (2009) and E. T. Meier & U. Shumlak (2012).

The electromagnetic field is evolved by the full Maxwell's equations

$$\frac{1}{c^2} \frac{\partial \mathbf{E}}{\partial t} + \mu_0 \mathbf{J} = \nabla \times \mathbf{B}, \quad (14)$$

$$\frac{\partial \mathbf{B}}{\partial t} = -\nabla \times \mathbf{E}, \quad (15)$$

akin to kinetic approaches. The fluid species and the electromagnetic field are coupled through the source terms on the right-hand-side of the momentum and energy equations. Resonant charge exchange between the ion and neutral populations is not included in this study. To assess its potential impact, we estimated the momentum transfer rates from both elastic collision and charge exchange using the charge exchange formulation from the multifluid MHD model in *J. Jara-Almonte et al. (2021)*. The two rates were found to be of the same order of magnitude. Thus, we argue that within the parameter regime investigated in this study, neglecting charge exchange is unlikely to alter the fundamental reconnection physics or scaling laws. In addition, electron-neutral collisions are also neglected due to their low rates and impact compared to ion-neutral collisions.

In this investigation, we set up the five-moment simulations to resemble those used by *J. Jara-Almonte et al. (2021)* but with some modifications. We work in the  $x$ - $y$  domain, with  $\hat{x}$  and  $\hat{y}$  being the inflow and outflow direction of the magnetic reconnection,  $\hat{z}$  being the out-of-plane direction. The neutral species was initialized as a uniform background at rest. An ionization fraction is defined by

$$\chi_0 = \frac{n_b}{n_n + n_b}, \quad (16)$$

where the number densities  $n_n$  and  $n_b$  correspond to the uniform neutral background and the ionized plasma, respectively (see below). The unperturbed plasma forms the Harris current sheet of thickness  $\delta$ , with number density and magnetic field,

$$n_i(x, y) = n_e(x, y) = n_b + n_0 \operatorname{sech}^2\left(\frac{y}{\delta}\right), \quad (17)$$

$$\mathbf{B}(x, y) = \hat{z} B_0 \tanh\left(\frac{y}{\delta}\right). \quad (18)$$

The total electric current,

$$\mathbf{J}(x, y) = \frac{1}{\mu_0} \nabla \times \mathbf{B}_0(x, y) = -\hat{z} \frac{B_0}{\mu_0 \delta} \frac{1}{\cosh^2(y/\delta)} \quad (19)$$

contains contributions from both electron and ion species due to the diamagnetic drift, so that  $J_{ze0}/J_{zi0} = T_{e0}/T_{i0}$ , where  $T_{e0}$  and  $T_{i0}$  are the uniform electron and ion temperature. In this investigation,  $T_{e0} = T_{i0} = T_0$ , though white noises are added to the electron temperature to break the initial configuration symmetry. A long-wavelength perturbation is imposed on the magnetic field,  $\delta\mathbf{B} = \hat{z} \times \nabla\delta\psi$ , to introduce a single X-line initially,

$$\delta\psi(x, y) = \delta\psi_0 \cos(2\pi x/L_x) \cos(\pi y/L_y). \quad (20)$$

Here,  $d_{i0} = \sqrt{m_i/(n_0 q^2 \mu_0)}$  denotes the ion inertial length associated with  $n_0$ . The characteristic parameters include  $m_n = m_i + m_e$ ,  $T_{n0} = T_{i0} = T_{e0} = T_0$ ,

and

$$\frac{m_i}{m_e} = 25, \quad \frac{\omega_{pe0}}{\Omega_{ce0}} = 2, \quad \beta_0 = \frac{2\mu_0 n_b T_0}{B_0^2} = 0.3, \\ n_b/n_0 = 0.3, \quad \frac{\delta}{d_{i0}} = 4, \quad \frac{\delta\psi_0}{B_0 d_{i0}} = 0.1. \quad (21)$$

Here, a thick initial current sheet is used to fully capture the thinning process.

The reference ion mean-free-path  $\lambda_{\text{mfp},\text{in}} \equiv (n_n \Sigma_{in})^{-1}$  is used to determine the constant collisional cross-section  $\Sigma_{in}$  indirectly. In this investigation, we will perform simulations with an electron-ion collision mean-free-path given by  $\lambda_{\text{mfp},\text{ei}}/d_{i0} = 40$  but varying

$$\frac{\lambda_{\text{mfp},\text{in}}}{d_{i0}} = 0.05, 0.5, 5, 50,$$

to cover strong to weakly ion-neutral coupling, and simultaneously varying initial ionization fraction

$$\chi_0 = 0.02, 0.04, 0.1, 0.2, 0.4, 0.8,$$

to span weakly to highly ionization regimes. A total of 24 runs were performed to cover the parameter matrix. The domain extends  $L_x \times L_y = 400d_{i0} \times 200d_{i0}$  and is discretized on a  $4096 \times 2048$  grid, with periodic and conducting wall boundary conditions at  $\hat{x}$  and  $\hat{y}$  boundaries, respectively. The above dimensionless parameters characterized the systems, though we further adopted unit normalizations for the numerical implementation such that  $\varepsilon_0 = \mu_0 = m_i = q_i = n_0 = 1$ .

### 3. SIMULATION RESULTS

The top row of Figure 1 gives an overview of the reconnection rate evolution. In the strongly collisional limit ( $\lambda_{\text{mfp},\text{in}}/d_{i0} = 0.05$ , top left panel), there is a clear stratification in reconnection rates based on ionization, with higher  $\chi_0$  leading to earlier onset times and higher peak reconnection rates. Conversely, as the ion-neutral collisionality decreases ( $\lambda_{\text{mfp},\text{in}}/d_{i0} = 50$ , top right panel), the system approaches a decoupled regime so that the temporal evolution and peak magnitude of the reconnection rates become largely insensitive to the ionization fraction. The onset time for fast reconnection in this five-moment model ranges from approximately  $1500$  to  $4700\Omega_{ci0}^{-1}$ . These timescales are comparable to those reported in previous multi-fluid MHD simulations but are significantly longer than the characteristic onset times of  $100$ - $200\Omega_{ci0}^{-1}$  typically observed in fully kinetic simulations by *J. Jara-Almonte et al. (2021, 2019)*. In addition to the inherent differences in onset between fluid and kinetic regimes, this discrepancy is likely largely attributable to the kinetic simulations being initialized with a thin current sheet with a half-thickness of  $d_{i0}$ .

The row 2-4 of Figure 1 shows the current layer structures from selected runs. In this strongly neutral-dominated regime ( $\chi_0 = 0.02$ , second row), decreasing

the collisionality (moving left to right) results in an increase in maximum outflow speeds and a transition in the current sheet structure, consistent with a transition from coupled to decoupled dynamics. At intermediate ionization ( $\chi_0 = 0.1$ , third row), structural changes are less significant. In the least collisional case (right panel), the early formation of secondary plasmoids becomes visible. In this three-fluid five-moment numerical investigation, dynamic plasmoid formation is generally more pronounced in low-collisionality or highly ionized runs during their nonlinear stages. For the highest ionization ( $\chi_0 = 0.8$ , bottom row), the outflow structure remains largely invariant across the range of collisionalities. This indicates that at high ionization fractions, the influence of ion-neutral collisions is negligible, and the system behaves similarly to the fully ionized limit.

The scaling of peak reconnection rate versus ionization fraction or ion-neutral collisionality are drawn in Figure 2. Figure 2a shows the ionization dependence. At high collisionality (low  $\lambda_{\text{mfp},\text{in}}/d_{i0}$ ), the reconnection rate is consistent with a scaling of  $\chi_0^{1/4}$ . As collisionality decreases, the rate transitions to a fast, ionization-independent regime characteristic of Hall-mediated reconnection.

Figure 2b examines the collisionality dependence. Generally, weaker ion-neutral coupling (higher  $\lambda_{\text{mfp},\text{in}}/d_{i0}$ ) enhances the reconnection rate. The  $\lambda_{\text{mfp},\text{in}}^{1/4}$  scaling observed up to  $\lambda_{\text{mfp},\text{in}}/d_{i0} \approx 5$  suggests an intermediate regime where ion-neutral friction plays a governing role. In the high ionization limit ( $\chi_0 = 0.8$ ), the rate becomes insensitive to collisionality, consistent with the fully ionized limit.

Next, we move to better understand the nature of onset, Figure 2c summarizes the critical current sheet half-thickness across various runs. In the strongly coupled regime, the current sheet thickness follows the  $\chi_0^{-1/4}$  scaling associated with the fully coupled Sweet-Parker theory. Conversely, in weakly coupled regimes, the thickness at onset stabilizes at a fraction of the ion inertial length ( $d_{i0}$ ), insensitive to  $\chi_0$ , which aligns with criteria for the onset of fast kinetic reconnection observed in previous PIC simulations.

Figure 3 illustrates the geometric properties of the current sheet during the fast reconnection phase. The current sheet half-thickness (Figure 3a) remains approximately  $0.3d_{i0}$  and is largely insensitive to the ionization fraction  $\chi_0$ . This value is thinner than the approximate value of  $0.8d_{i0}$  typically reported in fully kinetic PIC simulations, possibly due to the five-moment model's scalar pressure approximation lacking the full viscous dissipation provided by the non-gyrotropic pressure tensor. The current sheet length (Figure 3b) shows a weak dependence on  $\chi_0$ , which diminishes as the system becomes less collisional (increasing  $\lambda_{\text{mfp},\text{in}}/d_{i0}$ ). The lengths roughly range between  $2d_{i0}$  and  $10d_{i0}$ , largely consistent with kinetic simulations by J. Jara-Almonte

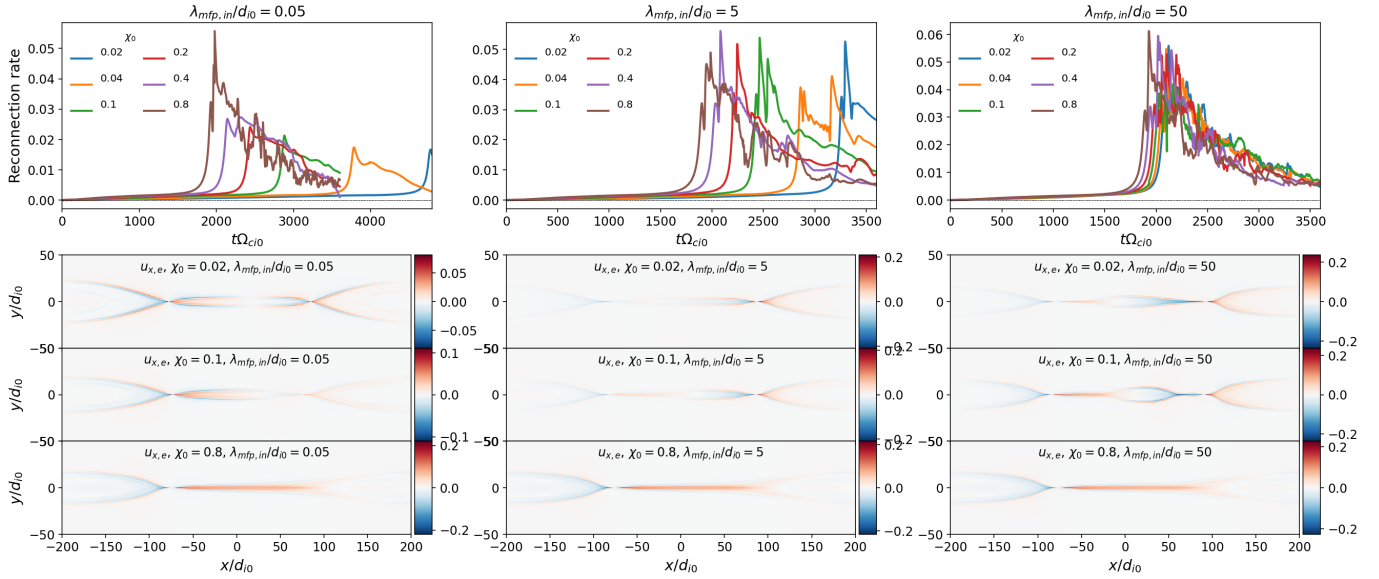
et al. (2021). These results contrast with previous multi-fluid simulations (e.g., (J. Jara-Almonte et al. 2021)), which observed a scaling where in-situ current sheet half-thickness and lengths,  $\delta_{\text{CS}}$  and  $L_{\text{CS}}$ , decrease with ionization like  $\chi^{-1/2}$  and  $\chi^{-3/4}$  respectively. The five-moment model appears to capture kinetic-like constraints on the current sheet aspect ratio that are absent in standard fluid models.

Figure 4 shows inflow and outflow cuts of ion/neutral velocities for runs with  $\chi_0 = 0.02$  (the most weakly ionized case), with ion-neutral collisionality decreasing from left to right. In the pre-onset phase (top two rows), the inflow region shows clear ion-neutral decoupling, a signature of ambipolar diffusion that promotes current-sheet thinning. In the lowest-collisionality run (right), the species are fully decoupled. Outflow coupling also depends strongly on collisionality, ranging from fully coupled (left) to decoupled (right), with the intermediate case ( $\lambda_{\text{mfp},\text{in}}/d_{i0} = 0.5$ ) showing strong coupling. In the peak reconnection phase (bottom two rows), accelerating reconnection enhances decoupling in both inflow and outflow regions. Notably, the intermediate-collisionality case transitions from coupled to decoupled outflows. Overall, across the explored ionization fractions and ion-neutral collisionalities, the three-fluid simulations exhibit a range of outflow coupling behaviors.

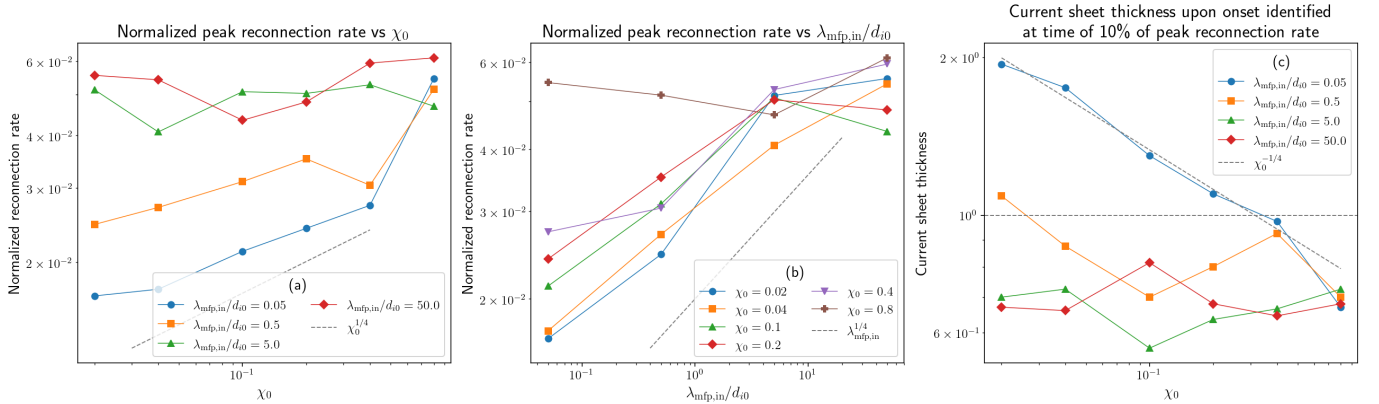
To further understand how ionization fraction influences the velocity coupling and physical regimes, Figure 5 shows the scaling of maximum ion (and hybrid) inflow (and outflow) velocities as functions of  $\chi$  for different ion-neutral collisionality. Here, the hybrid velocity is defined as the mass-weighted bulk velocity of ions and neutrals,  $\mathbf{u}_{\text{hybrid}} = (\rho_i \mathbf{u}_i + \rho_n \mathbf{u}_n) / (\rho_i + \rho_n)$ . For the most strongly coupled run set with  $\lambda_{\text{mpf},\text{in}}/d_{i0} = 0.05$  (blue curve in panel a), the ion outflow velocity scales like  $\chi^{1/2}$  when normalized by  $v_{A,\text{ion},\text{up}}$ , and is approximately 0.9-1 if normalized by  $v_{A,\text{hybrid},\text{up}}$  (not shown). In the most weakly coupled runs with  $\lambda_{\text{mpf},\text{in}}/d_{i0} = 50$  (red curve in panel b), the ion outflow velocity is about  $0.9v_{A,\text{ion},\text{up}}$ . In both limits, the ion outflow speed is therefore Alfvénic when measured relative to the appropriate effective Alfvén speed.

Figure 5b further shows that, for all collisionality sets, the hybrid outflow velocity scales approximately as  $\chi^{1/2}$  when normalized by  $v_{A,\text{ion},\text{up}}$ . In the strongly coupled limit, this behavior is consistent with the co-motion of ions and neutrals. As the coupling gets weaker, the  $\chi^{1/2}$  scaling largely persists, with larger deviations appearing only in the most weakly coupled run set (red curve). This indicates that the hybrid outflow velocity remains nearly independent of  $\chi$  when normalized by  $v_{A,\text{hybrid},\text{up}}$  over a broad range of collisionality.

Figure 5c and d show that the ion inflow velocity, when normalized by  $v_{A,\text{ion},\text{up}}$ , shows trends qualitatively similar to those of the outflow velocities in panels a and b. However, the inflow speeds display larger departures



**Figure 1.** Overview of the temporal evolution of reconnection rates and the spatial structure of electron outflows across the parameter space. (Top Row): Time-dependent reconnection rates normalized by the product of the asymptotic reconnecting magnetic field,  $B_0$ , and the ion Alfvén speed,  $v_{A0} = B_0/\sqrt{\mu_0 m_i n_b}$ . The rates are computed as the time derivative of the globally reconnected flux, i.e.,  $\max(\psi) - \min(\psi)$  along the midplane,  $\psi$  is the magnetic flux function. The columns correspond to runs with increasing ion-neutral collisionality, parameterized by the ratio of the mean free path to the ion inertial length,  $\lambda_{mfp,in}/d_{i0}$ . Within each panel, curves represent different initial ionization fractions,  $\chi_0$ . (Rows 2–4): 2D snapshots of electron outflow velocities (normalized by the speed of light) taken at the time of the first primary peak in the reconnection rate. Each row corresponds to a specific ionization fraction. Note that such primary peak times may precede the global maximum rate in cases where secondary plasmoid formation occurs later.



**Figure 2.** Scaling dependencies of the reconnection rate and current sheet geometry at onset. (a) Peak reconnection rate as a function of ionization fraction,  $\chi_0$ . Data points on the same curves represent the same ion-neutral collisionality,  $\lambda_{mfp,in}/d_{i0}$ . The dashed line indicates the theoretical  $\chi^{1/4}$  scaling for the resistive Sweet-Parker regime. (b) Peak reconnection rate as a function of the collisionality parameter,  $\lambda_{mfp,in}/d_{i0}$ , for fixed  $\chi_0$ . A  $\lambda_{mfp,in}^{1/4}$  reference scaling is provided. (c) Scaling of the critical current sheet half-thickness,  $\delta_{CS}$ , measured at the onset time (defined as 10% of the peak reconnection rate). The dashed slanted line represents the theoretical prediction for fully coupled fluids, while the horizontal dashed line marks the ion inertial length,  $d_{i0}$ .

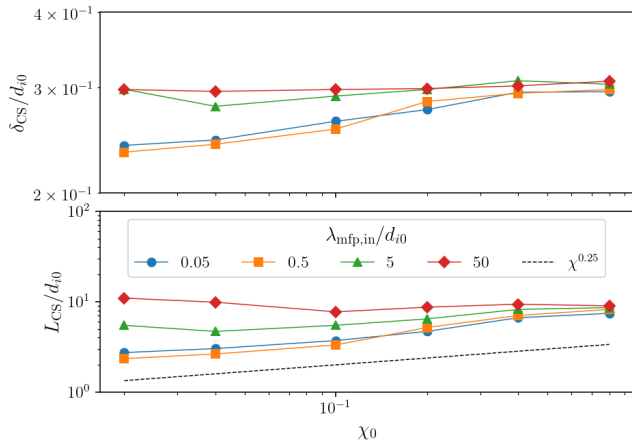


**Figure 3.** Dependence of current sheet morphology on ionization fraction and collisionality at the time of peak reconnection rate. (a) Current sheet half-thickness,  $\delta_{CS}$ , and (b) half-length,  $L_{CS}$ , plotted against the initial ionization fraction  $\chi_0$ . Dimensions are measured at the first primary peak of the reconnection rate to minimize effects from secondary island formation. The dashed line in panel (b) represents a  $\chi_0^{1/4}$  scaling.

from the  $\chi^{1/2}$  scaling, likely reflecting the stronger and persistent ion-neutral decoupling in the inflow region.

#### 4. DISCUSSION AND CONCLUSION

In this study, we employed a three-fluid five-moment model with separately evolved electrons, ions, and neutrals to investigate magnetic reconnection in partially ionized plasmas. By simultaneously scanning both the ion-neutral collisionality and ionization fraction, we examined the transition from strongly coupled, resistive reconnection to decoupled, Hall-mediated reconnection, and geometry constraints previously identified in kinetic simulations.

Unlike MHD-based models, the five-moment approach retains independent electron dynamics and associated effects beyond MHD (L. Wang et al. 2015; J. Ng et al. 2015). Our results show that in the weak coupling limit (large  $\lambda_{mfp,in}$ ), the five-moment fluid model reproduces several key kinetic features observed in PIC simulations (J. Jara-Almonte et al. 2019, 2021), while recovering fluid-theory predictions in well-coupled regimes.

A key finding of this work is the transition of the current sheet structure across coupling regimes. Analytic fluid theories (E. G. Zweibel et al. 2011; L. M. Malyshkin & E. G. Zweibel 2011) and multi-fluid MHD simulations (J. E. Leake et al. 2013; L. Ni et al. 2018) often predict that the ion diffusion region broadens to the hybrid scale  $d_i\chi^{-1/2}$  in the coupled regime, when ions and neutrals are well coupled. In contrast, our five-moment simulations show that the current sheet instead tends to thin to the ion-only inertial length  $d_i$ , largely independent of ionization fraction. This finding

is consistent with experimental results from MRX (E. E. Lawrence et al. 2013) and fully kinetic simulations (J. Jara-Almonte et al. 2019, 2021), suggesting that electron dynamics and other non-MHD effects could allow a fluid model to more faithfully capture the onset of fast reconnection.

These results help bridge the gap between computationally expensive kinetic approaches and large-scale fluid models. We demonstrate that the five-moment formulation can capture the transition to fast reconnection in partially ionized plasmas, a regime of importance in environments such as the solar chromosphere and protostellar disks. Future work could extend to a ten-moment model with tensorial pressure for each species. Electron pressure anisotropy and non-gyrotropy are known to influence reconnection in fully ionized plasmas (H. Ji et al. 2022), and viscous thermalization is expected to become important in the partially ionized regime by modifying the current-layer structure (J. Jara-Almonte et al. 2021). Another important extension is the inclusion of charge exchange, ionization, and recombination, which can dynamically regulate ion-neutral coupling, by, for example, acting as an effective plasma sink that facilitates inflow, thereby reshaping the current sheet and affecting the conditions required for fast reconnection.

Finally, it is important to note that earlier MRX experiments were thought to be limited by the device's small physical size, with restricted access to the decoupled regime ( $\nu_{ni}L/v_A^* < 1$ ). The upgraded and larger Facility for Laboratory Reconnection Experiments (FLARE) (H. Ji et al. 2022; H. Ji & W. Daughton 2011) can achieve higher Lundquist numbers and access ion-neutral coupling regimes that were previously out of reach. This presents a valuable opportunity for future laboratory tests of both fluid (MHD and moment-based) and kinetic predictions.

#### ACKNOWLEDGMENTS

The open-source code Gkeyll is publicly available at <https://github.com/ammarhakim/gkyl>. This work was partially supported by NSF grant AGS-2438328, AGS-2301337, AGS-2301338, DOE grant DE-SC0024639, NASA grant 80NSSC25K0050, the Alfred P. Sloan Research Fellowship, and IBM Einstein Fellow Fund at the Institute for Advanced Study, Princeton. We would like to acknowledge high-performance computing support from the Derecho system (doi:10.5065/qx9a-pg09) provided by the NSF National Center for Atmospheric Research (NCAR), sponsored by the National Science Foundation. We also would like to acknowledge high-performance computing support from National Energy Research Scientific Computing Center, a DOE Office of Science user facility, and the NASA High-End Computing (HEC) Program through the NASA Advanced Supercomputing (NAS) Division at Ames Research Center.

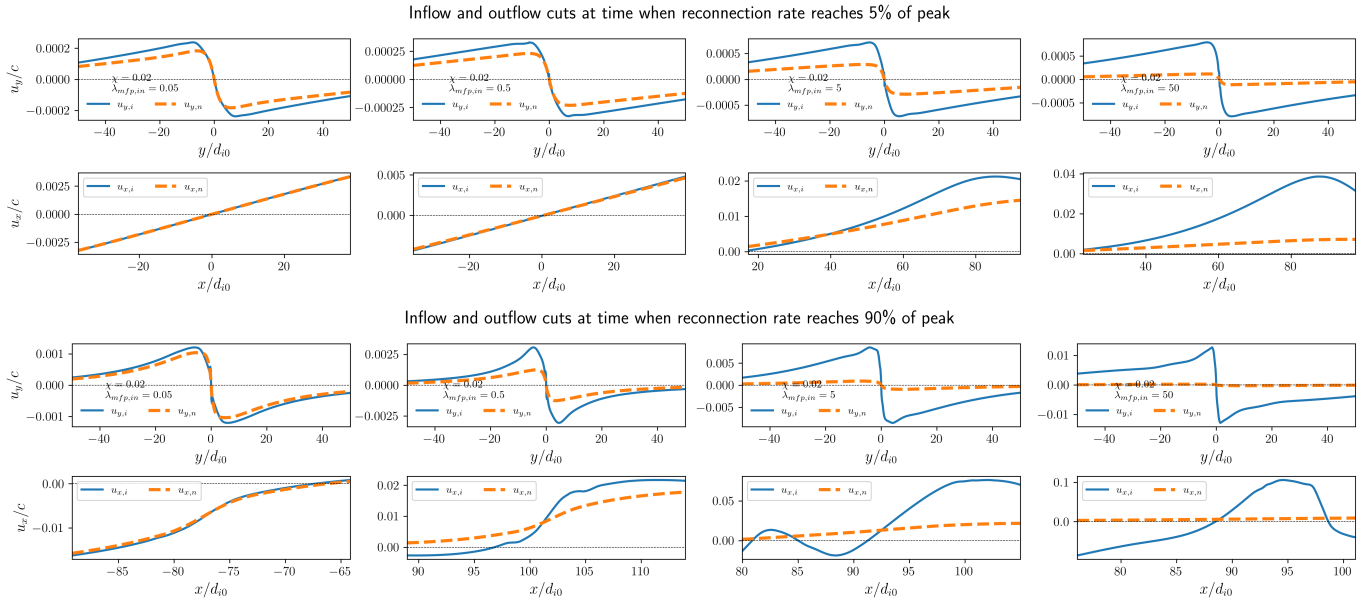


**Figure 4.** Spatial profiles of ion (blue solid) and neutral (orange dashed) inflow (first and third rows) and outflow (second and bottom rows) velocities in the vicinity of the X-point. (Top Two Rows) Velocity profiles taken at the pre-onset phase (5% of peak reconnection rate). (Bottom Two Rows) Velocity profiles taken during the fast reconnection phase (90% of peak rate). All panels display results for the low ionization case ( $\chi_0 = 0.02$ ), with ion-neutral collisionality decreasing from left to right ( $\lambda_{\text{mfp},\text{in}}/d_{i0}$  increasing).

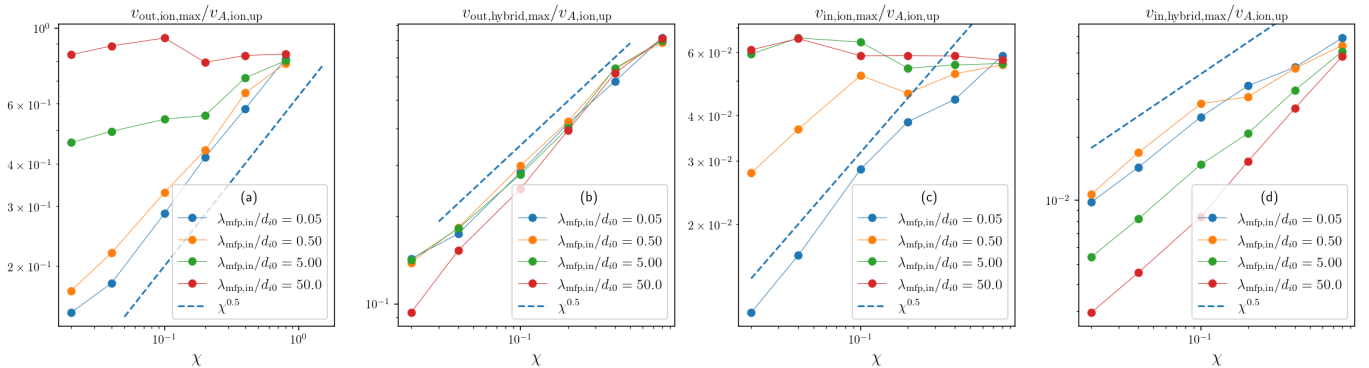


**Figure 5.** Scaling of maximum ion-only and hybrid-ion-neutral inflow/outflow velocities versus ionization fractions. Different lines correspond to run sets with different ion-neutral collisionality. The velocities are evaluated at the time of the first primary peak in each run, measured along inflow and outflow cuts through the primary X-point. All velocities are normalized to the initial asymptotic ion-only Alfvén speeds,  $v_{A,\text{ion},\text{up}}$ . Dashed lines indicate the reference  $\chi^{1/2}$  scaling.

## REFERENCES

- Fielding, D. B., Ripperda, B., & Philippov, A. A. 2023, *The Astrophysical Journal Letters*, 949, L5, doi: [10.3847/2041-8213/accf1f](https://doi.org/10.3847/2041-8213/accf1f)
- Hakim, A., Loverich, J., & Shumlak, U. 2006, *Journal of Computational Physics*, 219, 418
- Jara-Almonte, J., Ji, H., Yoo, J., et al. 2019, *Physical review letters*, 122, 015101
- Jara-Almonte, J., Murphy, N. A., & Ji, H. 2021, *Physics of Plasmas*, 28, 042108, doi: [10.1063/5.0039860](https://doi.org/10.1063/5.0039860)
- Ji, H., & Daughton, W. 2011, *Physics of Plasmas*, 18, doi: [10.1063/1.3647505](https://doi.org/10.1063/1.3647505)
- Ji, H., Daughton, W., Jara-Almonte, J., et al. 2022, *Nature Reviews Physics*, 4, 263, doi: [10.1038/s42254-021-00419-x](https://doi.org/10.1038/s42254-021-00419-x)
- Lawrence, E. E., Ji, H., Yamada, M., & Yoo, J. 2013, *Physical review letters*, 110, 015001
- Leake, J. E., Lukin, V. S., & Linton, M. G. 2013, *Physics of Plasmas*, 20

- Malyshkin, L. M., & Zweibel, E. G. 2011, *The Astrophysical Journal*, 739, 72, doi: [10.1088/0004-637x/739/2/72](https://doi.org/10.1088/0004-637x/739/2/72)
- Meier, E. T., & Shumlak, U. 2012, *Physics of Plasmas*, 19, doi: [10.1063/1.4736975](https://doi.org/10.1063/1.4736975)
- Ng, J., Huang, Y.-M., Hakim, A., et al. 2015, *Physics of Plasmas*, 22
- Ni, L., Ji, H., Murphy, N. A., & Jara-Almonte, J. 2020, *Proc. R. Soc. A*, 476
- Ni, L., Lukin, V. S., Murphy, N. A., & Lin, J. 2018, *The Astrophysical Journal*, 852, 95
- Schunk, R., & Nagy, A. 2009, *Ionospheres: Physics, Plasma Physics, and Chemistry*, Cambridge Atmospheric and Space Science Series (Cambridge Univ. Press), doi: [10.1017/CBO9780511635342](https://doi.org/10.1017/CBO9780511635342)
- Shibata, K., Nakamura, T., T. Matsumoto, K. O., et al. 2007, *Science*, 318, 1591
- Tian, H., DeLuca, E. E., Cranmer, S. R., et al. 2014, *Science*, 346, 1255711
- Wang, L., Hakim, A. H., Bhattacharjee, A., & Germaschewski, K. 2015, *Physics of Plasmas*, 22
- Wang, L., Hakim, A. H., Ng, J., Dong, C., & Germaschewski, K. 2020, *Journal of Computational Physics*, 415, 109510
- Yamada, M., Kulsrud, R., & Ji, H. 2010, *Rev. Mod. Phys.*, 82, 603
- Zweibel, E. G. 1989, *The Astrophysical Journal*, 340, 550, doi: [10.1086/167416](https://doi.org/10.1086/167416)
- Zweibel, E. G., Lawrence, E., Yoo, J., et al. 2011, *Physics of Plasmas*, 18, 111211, doi: [10.1063/1.3656960](https://doi.org/10.1063/1.3656960)
- Zweibel, E. G., & Yamada, M. 2009, *Annu. Rev. Astron. Astrophys.*, 47, 291–332
- Öberg, K. I., Qi, C., Wilner, D. J., & Andrews, S. M. 2011, *The Astrophysical Journal*, 743, 152, doi: [10.1088/0004-637X/743/2/152](https://doi.org/10.1088/0004-637X/743/2/152)